MULTIBODY DYNAMICS 2011, ECCOMAS Thematic Conference
J.C. Samin, P. Fisette (eds.)
Brussels, Belgium, 4-7 July 2011

SIMULATION OF INDETERMINATE MULTI-POINT IMPACT AND CONTACT WITH FRICTION

Adrian Rodriguez[⋆] **and Alan Bowling**[†]

[⋆]Department of Mechanical and Aerospace Engineering
University of Texas at Arlington, Arlington, TX 76017 USA
e-mail: adrianrodriguez2009@mavs.uta.edu,

[†]Department of Mechanical and Aerospace Engineering
University of Texas at Arlington, Arlington, TX 76017 USA
e-mail: bowling@uta.edu

Keywords: Indeterminate, Simultaneous, Multi-Point Impact, Velocity Constraints.

Abstract. *This work presents a method for determining the post-impact behavior of a rigid body undergoing multiple, simultaneous impacts with friction. A discrete algebraic model is used with an event-driven function which finds impact events. In this work, the indeterminate nature of the equations of motion encountered at impact is examined. A velocity constraint is developed based on the rigid body assumption to address the equations and an impact law is used to determine the impulsive forces. The slip-state of each contact point is then determined and appropriate methods are used to resolve the post-impact velocities. These techniques are applied to a planar model of a ball which is forced to impact a corner between the ground and a wall. Simulations are presented to demonstrate the post-impact behavior of the ball experiencing simultaneous, multiple impacts with friction.*

1 INTRODUCTION

This paper proposes a new approach to investigate the modeling and simulation of multiple, simultaneous impact and contact with friction on a single rigid body. The equations of motion for these systems are indeterminate meaning that the number of impact forces are more than the number equations available. These impact forces must be solved to determine the slip-state of each contact point, which allows a prediction of the post-impact behavior of the system.

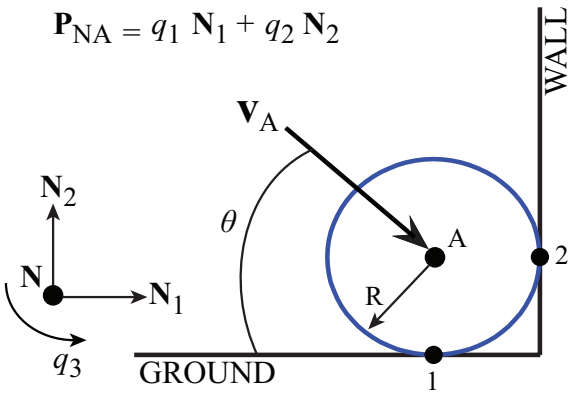

Figure 1: Planar model of a ball.

The test case used here is a planar model of a ball with radius R, shown in Fig. 1. The ball has three degrees-of-freedom (DOFs) denoted by generalized coordinates q_1 and q_2 which are translational and q_3 is rotational. The ball's position is indicated by the position vector $\mathbf{P_{NA}}$ and θ is the angle of impact. At the point of impact, the ball is in simultaneous contact with the ground, point 1, and the wall, point 2. Two force components are present at each impact point, F_1-F_4 as shown in Fig. 2. One force is normal to both surfaces, and the other is tangential to both surfaces and is caused by friction.

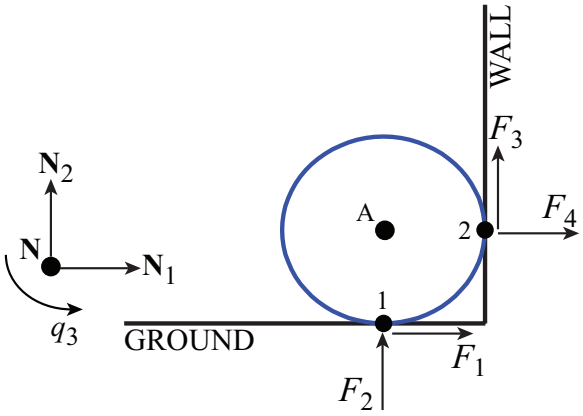

Figure 2: Contact forces at impact.

The paper is organized as follows. Background will be presented on the various approaches which have been pursued to address contact indeterminacy. The development of a velocity constraint based on the rigid body assumption will be given followed by a brief discussion of

the derivation of an impact law which uses the velocity constraint. Then, the theory used to resolve the post-impact velocities of the system and the simulation results will be presented.

2 BACKGROUND

The classical treatment of rigid body collisions has been extensively studied to model and examine multiple point contact with friction [1, 2, 3]. A discontinuous approach is used in this work which splits the impact event into two regions: before impact and after impact. This method assumes that the position and orientation of the body does not change during the impact event which occurs over a very short time period [4].

The integrator used in the simulation is Matlab's ode45.m along with an event function that captures when an impact event has occurred. The post-impact velocities are calculated algebraically and serve as the initial conditions when the simulation is restarted. In this work, a discrete algebraic model is used with the development of an impact law as in [5] that examines the impulses and momenta of the system.

Dynamic modeling of systems involving simultaneous, multiple impacts with friction yield equations of motion which are indeterminate with respect to the impact forces [1, 6, 7, 8]. This indeterminacy is caused by a non-square Jacobian, which is not invertible, and premultiplies the impact forces in the equations of motion. This is problematic because the impact forces are needed to determine the state of sticking or slipping at each impact and contact point. There are methods available which have been used in the literature for addressing this situation. One simple method is to add more degrees-of-freedom to the problem by considering elasticity in the bodies [1]. This is in contrast to rigid body approaches, which directly consider the properties of the non-square Jacobian.

For example, in [6], the QR factorization is used to determine the impact force components which have the least effect on the system according to the elements in the factorization. The impact forces having the least effect on the dynamics are removed, set equal to zero, in order to allow a solution for the remaining components. In other work, indeterminate contact forces are encountered for robotic manipulators when multiple contact points are involved in grasping an object [7, 8]. These works examine the static friction forces present at the contact points and determine the infeasibility of some solutions. The authors intuitively develop force constraints based on the situation-specific contact geometry of the grasped object to solve the indeterminate equations. These methods are useful and provide a reasonable means to address the indeterminacy of the equations.

In this work, an effort is made to develop a more general approach to addressing contact force indeterminacy than in [7, 8], by using a velocity constraint that is more consistent with the assumptions which form the basis for classical rigid body impact analysis, in contrast to [6]. Any point on a rigid body by definition remains the same distance from all the other points on the body assuming that no deformations take place [9]. Hence, it is possible to formulate a relationship between the impact points on the rigid body and express it in terms of velocities. This development is applied in the derivation of an impact law which is used to calculate the impulsive forces associated with impact [4, 10]. The post-impact velocities can then be computed to simulate the post-impact behavior of the system.

3 RESOLVING INDETERMINACY

Examination of the impulsive forces requires consideration of the impact forces in the equations of motion,

$$A\,\ddot{\mathbf{q}} + \mathbf{g}(\mathbf{q}) \;=\; \mathbf{\Gamma}(\mathbf{q}) \;=\; J^T(\mathbf{q})\,\mathbf{F} \tag{1}$$

where A is the mass matrix, $\mathbf{\Gamma}$ contains the generalized active forces, and J is a Jacobian matrix that defines the velocity and forces at the impact points. The generalized coordinates are included in $\mathbf{q}$, while $\mathbf{g}$ and $\mathbf{F}$ are vectors of gravity and impact forces, respectively.

For the planar ball considered in this work, there are no external forces acting on the body. The equations of motion for this system take the form of,

$$A \begin{bmatrix} \ddot{q}_1 \\ \ddot{q}_2 \\ \ddot{q}_3 \end{bmatrix} + \mathbf{g}(\mathbf{q}) \;=\; \mathbf{\Gamma}(\mathbf{q}) \;=\; J^T \begin{bmatrix} F_1 \\ F_2 \\ F_3 \\ F_4 \end{bmatrix} \tag{2}$$

This gives three equations but four unknown forces defined by F_1-F_4, resulting in equations which are indeterminate with respect to these impact forces.

3.1 Velocity Constraints

Here, the theory of rigid body dynamics will be examined in order to address the indeterminacy in (2). It is assumed that any deformations occurring during the impact are small enough to be neglected. Therefore, the distance between a point on the body will remain the same distance from all the other points on the body [9]. This idea can be used to examine the relationship between velocities at different points on a rigid body. Consider the planar ball illustrated in Fig. 3 with angular velocity, $\boldsymbol{\omega}$ and where the impact forces have been replaced by normal and tangential velocity components. If the velocity of the ball's center of mass at point A is known,

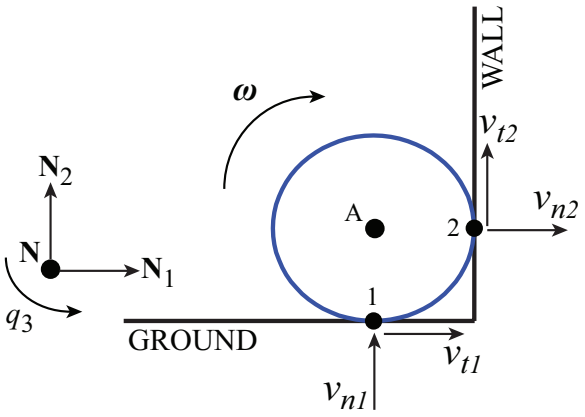

Figure 3: Velocity components at the contact points.

$\mathbf{v_A}$, with respect to an inertial reference frame, then the velocity of point 1 and 2 can be found as,

$$\begin{aligned} \mathbf{v_1} &= \mathbf{v_A} + \mathbf{v_{A1}} \\ \mathbf{v_2} &= \mathbf{v_A} + \mathbf{v_{A2}} \end{aligned} \tag{3}$$

where $\mathbf{v_{A1}}$ is the relative velocity between points A and 1 and $\mathbf{v_{A2}}$ is the relative velocity between points A and 2 [9].

Eliminating $\mathbf{v_A}$ from the relations in (3) yields

$$\begin{aligned} \mathbf{v_2} - \mathbf{v_1} &= \mathbf{v_{A2}} - \mathbf{v_{A1}} \\ &= \boldsymbol{\omega} \times (\mathbf{P_{A2}} - \mathbf{P_{A1}}) \\ &= \boldsymbol{\omega} \times \mathbf{P_{12}} \end{aligned} \tag{4}$$

The terms $\mathbf{v_1}$ and $\mathbf{v_2}$ in (4) contain the normal and tangential velocities of the impact points such that,

$$\begin{bmatrix} v_{n2} \\ v_{t2} \\ 0 \end{bmatrix} - \begin{bmatrix} v_{t1} \\ v_{n1} \\ 0 \end{bmatrix} = \begin{bmatrix} -R\,\dot{q}_3 \\ R\,\dot{q}_3 \\ 0 \end{bmatrix} \tag{5}$$

where the subscripts n and t distinguish between normal and tangential velocities. The first two equations in (5) can be summed to eliminate the generalized coordinate

$$v_{n2} + v_{t2} - v_{t1} - v_{n1} = 0 \tag{6}$$

which yields a relationship between the velocities at the impact points.

In this way, the rigid body assumption has allowed for the definition of a constraint which can be applied to the equations of motion to make them determinate. This procedure will be demonstrated in the following section.

3.2 Constraint Implementation

The dual nature of the impact Jacobian expresses the relationship between velocities and forces,

$$\boldsymbol{\vartheta} = \begin{bmatrix} \mathbf{v_1} \\ \mathbf{v_2} \end{bmatrix} = J\,\dot{\mathbf{q}}\,, \qquad \boldsymbol{\Gamma} = J^T\,\mathbf{F} = J^T \begin{bmatrix} F_1 \\ \vdots \\ F_4 \end{bmatrix} \tag{7}$$

The velocity constraint obtained in (6) will be used to constrain one of the tangential velocities. Consider an example where v_{t1} is constrained. This is accomplished by solving for this velocity in the constraint equation and substituting the expression which gives,

$$\boldsymbol{\vartheta} = \begin{bmatrix} v_{t1} \\ v_{n1} \\ v_{t2} \\ v_{n2} \end{bmatrix} = \begin{bmatrix} -v_{n1} + v_{t2} + v_{n2} \\ v_{n1} \\ v_{t2} \\ v_{n2} \end{bmatrix} = z^*\,\boldsymbol{\vartheta}^* \tag{8}$$

where z^* is a permutation matrix containing the velocity constraint and $\boldsymbol{\vartheta}^*$ contains the unconstrained velocities.

The dual nature of the Jacobian also defines a relationship between unconstrained velocities and forces, $\mathbf{F}^*$, as in (7)

$$\boldsymbol{\vartheta}^* = J^*\,\dot{\mathbf{q}} \qquad \boldsymbol{\Gamma} = J^{*T}\,\mathbf{F}^* \tag{9}$$

Combining expressions from (7), (8), and (9) yields

$$\boldsymbol{\vartheta} = J\,\dot{\mathbf{q}} = z^*\,\boldsymbol{\vartheta}^* = z^*\,J^*\,\dot{\mathbf{q}} \tag{10}$$

where J^* is the constrained Jacobian matrix such that,

$$J \;=\; z^*\; J^* \qquad\qquad J^T \;=\; J^{*T}\; z^{*T} \tag{11}$$

which gives the relationship between the original Jacobian and the constrained Jacobian. The inverse relations for (11) have the form

$$z\; J \;=\; J^* \qquad\qquad J^T\; z^T \;=\; J^{*T} \tag{12}$$

where z is the left-inverse of z^*,

$$z = (z^{*T}\; z^*)^{-1}\; z^{*T} \tag{13}$$

Relations from (7), (9), and (12) are used to obtain

$$\mathbf{\Gamma} \;=\; J^T\; \mathbf{F} \;=\; J^{*T}\; \mathbf{F}^* \;=\; J^T\; z^T\; \mathbf{F}^* \tag{14}$$

which defines the following relation

$$\mathbf{F} \;=\; z^T\; \mathbf{F}^* \tag{15}$$

The relation in (9) and (14) can be used in (1) to give,

$$A\; \ddot{\mathbf{q}} + \mathbf{g}\;(\mathbf{q}) \;=\; \mathbf{\Gamma} \;=\; J^{*T}\; \mathbf{F}^* \tag{16}$$

which represents the equations of motion in a form that is determinate with respect to the unconstrained forces. This model, (15) and (16), will be used to calculate the impulsive forces and evaluate the slip-state at the impact points.

4 DETERIMINING POST-IMPACT VELOCITIES

For the case in the normal direction, the post-impact velocity is simply determined with the use of Newton's COR which is a function of the normal velocity before impact. Hence, the post-impact normal velocity takes the form of,

$$v_{n_i}(t+\epsilon) = -e_{n_i} v_{n_i}(t) \tag{17}$$

such that $0 \leq e_{n_i} \leq 1$ and $e_{n_i} \neq 0$ is used to model rebound.

The post-impact tangential velocities are found using a two step process which first involves determining the impulsive forces at each impact point. Knowing these forces allows the determination of the slip-state at each point using the complementarity conditions [11, 12]. However, these conditions do not provide a unique solution to the post-impact velocities if any of the impact points slip [5]. Thus, a maximum dissipation principle is used herein to find a unique solution to the post-impact velocities.

4.1 Impulsive Forces

Definite integration of (16) over a short time ϵ,

$$\int_t^{t+\epsilon} \left(A\; \ddot{\mathbf{q}} + \mathbf{g}\;(\mathbf{q})\right)\, dt = \int_t^{t+\epsilon} J^{*T}(\mathbf{q})\; \mathbf{F}^*\; dt \tag{18}$$

gives,

$$A\; (\; \dot{\mathbf{q}}(t+\epsilon) - \dot{\mathbf{q}}(t)\;) = J^{*T}\; \mathbf{p}^* \tag{19}$$

Multiplying the inverse of the mass matrix on each side,

$$\dot{\mathbf{q}}(t+\epsilon) - \dot{\mathbf{q}}(t) = A^{-1}\, J^{*T}\, \mathbf{p}^* \tag{20}$$

in which m $\leq$ n making it an underconstrained system of equations. The two unknowns in (20) are $\dot{\mathbf{q}}(t+\epsilon)$ and $\mathbf{p}^*$. Not all of the terms in $\dot{\mathbf{q}}$ contribute to the impact forces contained in $\mathbf{p}^*$. The contributing terms in $\dot{\mathbf{q}}$ can be expressed as the velocities of the impact points using the expression in (9),

$$\boldsymbol{\vartheta}^*(t+\epsilon) - \boldsymbol{\vartheta}^*(t) = J^*\, A^{-1}\, J^{*T}\, \mathbf{p}^* \tag{21}$$

resulting in a one-to-one mapping between the velocities and forces involved at impact. Solving for $\mathbf{p}^*$ gives,

$$\left(J^* A^{-1} J^{*T}\right)^{-1} \left(\boldsymbol{\vartheta}^*(t+\epsilon) - \boldsymbol{\vartheta}^*(t)\right) = \mathbf{p}^* \tag{22}$$

The impulsive forces for all impact points can be obtained from (15) as,

$$\mathbf{p} \;=\; z^T\, \mathbf{p}^* \tag{23}$$

Thus, the impulsive forces can be expressed as,

$$\mathbf{p} = z^T\, \left(J^* A^{-1} J^{*T}\right)^{-1} (\boldsymbol{\vartheta}^*(t+\epsilon) - \boldsymbol{\vartheta}^*(t)) \tag{24}$$

The formulation above demonstrates the determination of all of the impulsive forces at impact.

4.2 Maximum Dissipation Principle

Here optimization techniques are used to find a unique solution for the post-impact velocities. It is formulated using the no-slip condition given in the complementarity conditions. The no-slip condition is modified as,

$$\frac{\|\mathbf{p}_{t_i}\|}{|\mathrm{p}_{n_i}|} \;\geq\; \mu_i(\boldsymbol{\vartheta}^*(t+\epsilon)) \tag{25}$$

where the static coefficient of friction has been replaced by a general one, and

$$\begin{cases} 0 \;\leq\; \mathrm{p}_{n_i} & \text{ground contact} \\ 0 \;\geq\; \mathrm{p}_{n_i} & \text{wall contact} \end{cases} \tag{26}$$

for $i \in \{1, \ldots, m\}$. The condition in (26) ensures that the impacting point does not penetrate the surface. The μ_i obtained in (25) is calculated using the tangential and normal impulsive forces, $\mathbf{p}_{t_i}$ and p_{n_i}, which are functions of $\boldsymbol{\vartheta}^*(t+\epsilon)$.

The dissipation principle used here considers the coefficients of friction and restitution and determines their feasibility. If these coefficients are found to be infeasible, then the dissipation principle ensures a feasible μ is achieved. This is accomplished by minimizing the distance $\mathbf{d}$ from the known solution to the no-slip solution, as in [13],

$$\mathbf{d} \;=\; \begin{bmatrix} \mu_s \\ 0 \\ \mu_s \end{bmatrix} - \begin{bmatrix} \mu_1 \\ v_{t,1}(t+\epsilon) \\ \mu_2 \end{bmatrix} \tag{27}$$

subject to the no-slip condition which allows expressions for the nonconvex feasible region as,

$$\min_{(v_{t,i}(t+\epsilon))} \qquad \text{obj} \;:=\; \mathbf{d}^T\,\mathbf{d} \tag{28}$$

subject to

$$\mathbf{p}_{t_i}^T\,\mathbf{p}_{t_i} - \mu_i^2\;\mathrm{p}_{n_i}^2 \;\geq\; 0 \tag{29}$$

$$\begin{cases} 0 \;\leq\; \mathrm{p}_{n_i} & \text{ground contact} \\ 0 \;\geq\; \mathrm{p}_{n_i} & \text{wall contact} \end{cases} \tag{30}$$

where,

$$z^T\;\left(J^* A^{-1} J^{*T}\right)^{-1}\left(\boldsymbol{\vartheta}^*(t+\epsilon) - \boldsymbol{\vartheta}^*(t)\right) = \;\mathbf{p} \tag{31}$$

$$\min\left(\mu_d,\;\mu_{f_i}\right) \;=\; \mu_{min_i} \tag{32}$$

$$\mu_{min_i} \;+\; \left(\mu_s - \mu_{min_i}\right)\;\mathrm{e}^{-\left(\frac{\|v_{t_i}\|}{v_s}\right)^a} \;=\; \mu_i \tag{33}$$

for $i \in \{1,\ldots,m\}$. The objective function used here performs like a maximum dissipation principle by minimizing the value of the tangential velocity. The constraint in (32) ensures the smaller quantity between μ_d and μ_{f_i} is used in the Karnopp model in (33), which helps smooth the transition between the sticking and slipping regions [14]. The value of μ_{f_i} corresponds to the coefficient of friction when $v_{t_i} = 0$ for no-slip contact. For this work, $v_s = 1.4 \times 10^{-4} m/s$ and a = 1 such that when $\|v_{t_i}\| \approx 1 \times 10^{-3},\ \mu_i \approx \mu_{min}$. Similarly, when $\|v_{t_i}\| \approx 0,\ \mu_i \approx \mu_s$. Using this formulation, the feasible post-impact tangential velocity of each impact point can be resolved.

5 RESULTS

Here, two simulations of the planar ball in Fig. 1 impacting a corner, as in Fig. 2, using different angles of impact are performed to show that the proposed method yields a unique solution for the post-impact velocities. In Sec. 3.1 a constraint equation was obtained in which two tangential velocities appeared in the constraint. This allows elimination of one tangential velocity from the two available in (8); the post-impact normal velocities are already defined using the COR in (17). A static and dynamic coefficient of friction of 0.5 and 0.25 are used in both examples. There is no rationale for choosing which tangential velocity to eliminate, so here both cases are examined in each example to ensure that they each yield a unique solution.

5.1 Example 1: Angle of Impact, $\theta \approx 30^\circ$

The initial, pre-impact, and post-impact states of the ball are presented in Table 1. The ball was given an initial position and translational velocity but no angular velocity.

The simulation of the ball is depicted as it impacts a corner defined by the ground and a wall and ends when a second impact is captured with the ground, as shown in Fig. 4. After impacting the corner, the angular rotation of the ball demonstrates the positive angular velocity gained as a result of impact. This angular velocity can be attributed to the ground contact point sticking while the wall contact point slips.

Table 1: Simulation results for $\theta \approx 30^\circ$

	Initial	Pre-impact	Post-impact
Position			
q_1	0.0 m	3.614 m	3.614 m
q_2	1.5 m	0.500 m	0.500 m
q_3	0.0 rad	0.0 rad	0.0 rad
Velocity			
$\dot{q}_1$	8.0 m/s	8.0 m/s	-4.0 m/s
$\dot{q}_2$	0.0 m/s	-4.430 m/s	2.215 m/s
$\dot{q}_3$	0.0 m/s	0.0 m/s	8.0 m/s

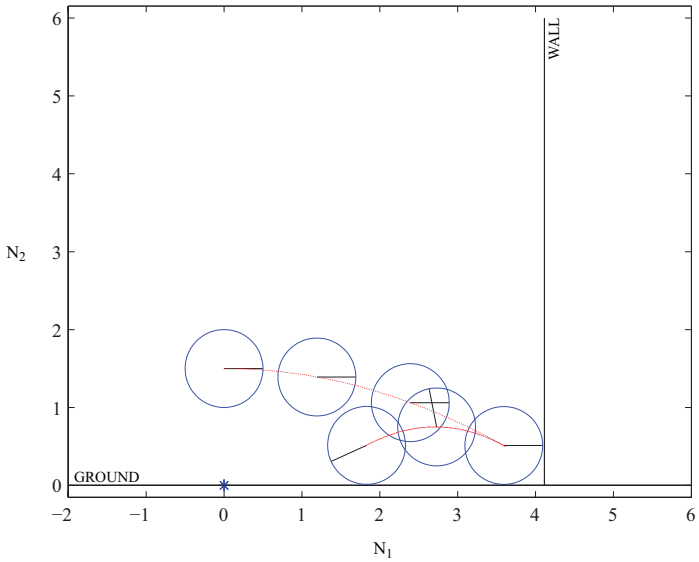

Figure 4: Simulation results for $\theta \approx 30^\circ$.

The trajectory of the ball's mass center throughout the simulation is shown in Fig. 4 by the curve. After impact, the ball follows a lower trajectory which suggests that the system lost energy from the impact. It is possible that a system may gain energy from an impact based on the methods used in this work to obtain a solution for the post-impact velocities. The potential, kinetic, and total energy was examined throughout the simulation, as shown in Fig. 5, to ensure that no energy gains were encountered. At the point of impact, it can be seen that the total energy of the system decreases significantly which is consistent for an impact.

5.2 Example 2: Angle of Impact, $\theta \approx 60^\circ$

In this case, the ball was given a higher initial position and smaller translational velocity but still no angular velocity. The initial, pre-impact, and post-impact states of the ball for this example are presented in Table 2.

The simulation of the ball, similar to Example 1, is shown in Fig. 6. In this example, the ball is depicted as gaining a negative angular velocity from impact. This angular velocity is a direct result of the ground contact point slipping while the wall contact point sticks.

The trajectory of the ball's mass center throughout the simulation is shown in Fig. 6 by

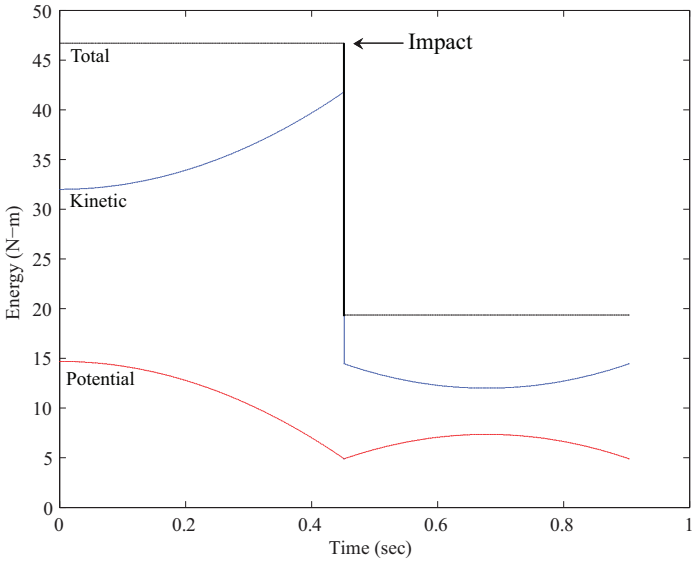

Figure 5: Energy consistency for $\theta \approx 30°$.

Table 2: Simulation results for $\theta \approx 60°$

	Initial	Pre-impact	Post-impact
Position			
q_1	0.0 m	3.833 m	3.833 m
q_2	5.0 m	0.500 m	0.500 m
q_3	0.0 rad	0.0 rad	0.0 rad
Velocity			
$\dot{q}_1$	4.0 m/s	4.0 m/s	-2.0 m/s
$\dot{q}_2$	0.0 m/s	-9.391 m/s	4.696 m/s
$\dot{q}_3$	0.0 m/s	0.0 m/s	-7.823 m/s

the curve. Once again, the ball follows a lower trajectory after impact. The potential, kinetic, and total energy was examined throughout the simulation to ensure there were no energy gains, as shown in Fig. 7. The total energy of the system decreases at the point of impact which is consistent for an impact.

6 CONCLUSIONS

In this work, the post-impact behavior of a planar ball in simultaneous, multi-point contact with friction was examined. The equations of motion of the system were indeterminate with respect to the impact forces. A velocity constraint based on the rigid body assumption was developed and applied to the equations to make them determinate. The use of the velocity constraint was consistent with the concepts related to the treatment of collisions in classical rigid body mechanics. It was shown that this constraint, in conjunction with a maximum dissipation principle, led to a determination of a unique solution for the post-impact velocities. It was also shown that this technique led to a solution that was energetically consistent in terms of the fact that impact should not increase the system's total energy. Although a planar system was considered here, the proposed technique should be applicable to a three dimensional system which experiences multiple impacts.

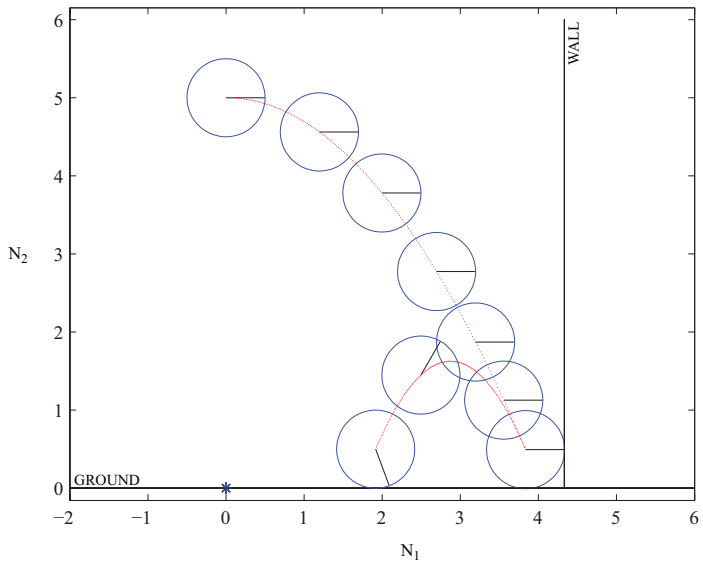

Figure 6: Simulation results for $\theta \approx 60°$.

REFERENCES

[1] Y.-T. Wang, V. Kumar, and J. Abel, "Dynamics of rigid bodies undergoing multiple frictional contacts," *Proceedings-IEEE International Conference on Robotics and Automation*, vol. 3, pp. 2764–2769, May 1992.

[2] L. Johansson, "A linear complementarity algorithm for rigid body impact with friction," *European Journal of Mechanics, A/Solids*, vol. 18, no. 4, pp. 703–717, Jul. 1999.

[3] D. E. Stewart, "Rigid-body dynamics with friction and impact," *SIAM Review*, vol. 42, no. 1, pp. 3–39, Mar. 2000.

[4] G. Gilardi and I. Sharf, "Literature survey of contact dynamics modelling," *Mechanism and Machine Theory*, vol. 37, no. 10, pp. 1213–1239, Oct. 2002.

[5] A. Bowling, D. M. Flickinger, and S. Harmeyer, "Energetically consistent simulation of simultaneous impacts and contacts in multibody systems with friction," *Multibody System Dynamics*, vol. 22, no. 1, pp. 27–45, Aug. 2009.

[6] L. Johansson, "A newton method for rigid body frictional impact with multiple simultaneous impact points," *Computer Methods in Applied Mechanics Engineering*, vol. 191, pp. 239–254, Nov. 2001.

[7] Y. Maeda, K. Oda, and S. Makita, "Analysis of indeterminate contact forces in robotic grasping and contact tasks," *IEEE International Conference on Intelligent Robots and Systems*, pp. 1570–1575, Oct. 2007.

[8] T. Omata and K. Nagata, "Rigid body analysis of the indeterminate grasp force in power grasps," *IEEE Transactions on Robotics and Automation*, vol. 16, no. 1, pp. 46–54, Feb. 2000.

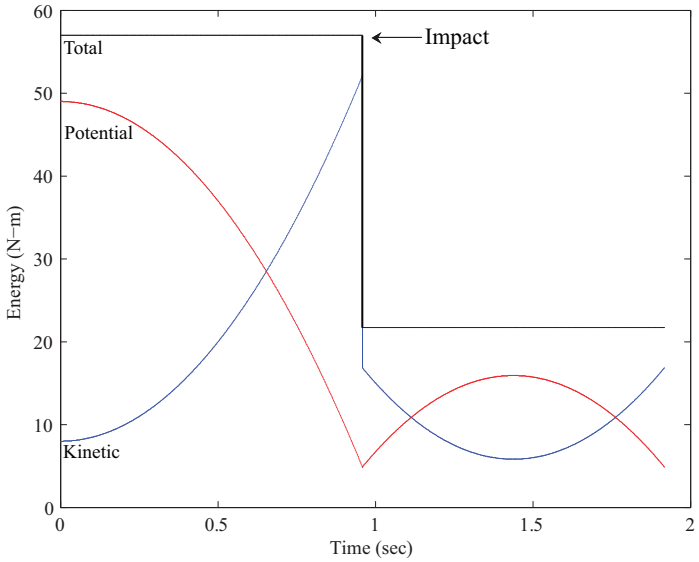

Figure 7: Energy consistency for $\theta \approx 60°$.

[9] A. Bedford and W. Fowler, *Engineering Mechanics: Dynamics*. Pearson Education, Inc., 2008.

[10] S. Djerassi, "Collision with friction; part b: Poisson's and stornge's hypotheses," *Multibody System Dynamics*, vol. 21, no. 1, pp. 55–70, Feb. 2009.

[11] L. Johansson and A. Klarbring, "Study of frictional impact using a nonsmooth equations solver," *Journal of Applied Mechanics*, vol. 67, no. 2, pp. 267–273, Jun. 2000.

[12] C. Glocker and C. Studer, "Formulation and preparation for numerical evaluation of linear complementarity systems in dynamics," *Multibody System Dynamics*, vol. 13, no. 4, pp. 447–463, May 2005.

[13] D. M. Flickinger and A. Bowling, "Simultaneous oblique impacts and contacts in multibody systems with friction," *Multibody System Dynamics*, vol. 23, no. 3, pp. 249–261, Mar. 2010.

[14] D. Karnopp, "Computer simulation of stick-slip friction in mechanical dynamic systems," *Journal of Dynamic Systems, Measurement and Control, Transactions of the ASME*, vol. 107, no. 1, pp. 100–103, Mar. 1985.